A piezo-based rotational inertia shaker for the active control of rotating machinery

G. Zhao[1], G. Pinte[2], S. Devos[2], J. Swevers[1], P. Sas[1]
[1] KU Leuven, Department Mechanical Engineering
Celestijnenlaan 300 B, B-3001, Heverlee, Belgium
e-mail: **guoying.zhao@mech.kuleuven.be**

[2] Flanders MECHATRONICS Technology Centre
Celestijnenlaan 300 D, B-3001, Heverlee, Belgium

Abstract
This paper presents an axisymmetric rotational inertia shaker for reducing the structure borne noise radiated by rotating machinery. This modular inertia shaker uses a piezostack to generate a compensating force on a rotating element by accelerating a ring shaped mass. The piezostack is controlled using an adaptive shunt circuit, which emulates the impedance of a variable inductance. The inertia shaker is tested on an experimental test bed where a disturbance force excites a rotating shaft, which is mounted in a frame. As a result, noise is radiated by a plate that is attached to the frame. The performance of the inertia shaker is first evaluated during non-rotating tests. When the virtual inductance is tuned optimally, a shaft vibration reduction of more than 12 dB and a corresponding noise reduction of 9 dB are obtained. Afterwards, the performance has also been checked during a rotating test. A comparable reduction as in the non-rotating tests is obtained when the piezostack is in the same direction as the disturbance force, while there is nearly no reduction when the piezostack is in the perpendicular direction to the disturbance.

1 Introduction

Due to the increasing attention for the environmental impact of newly developed machines, noise radiation is becoming an important competitive quality for rotating machinery such as gearboxes and compressors. To decrease the noise level in these industrial applications to the desired level, passive techniques such as sound absorption or isolation alone are no longer sufficient [1]. Therefore, nowadays active solutions are explored to reduce the noise radiation level in rotating machines.

Depending on the location where the active element operates in a vibration propagation path, two active control approaches can be distinguished. In a first approach, the vibro-acoustic response of the radiating surfaces is controlled by active means. Typical examples are smart panels [2] with piezoelectric patches to control the noise radiating surfaces of a housing. Alan R. Masters et al. [3] demonstrated the feasibility of active control of compressor noise radiation by using piezoelectric patch actuators which are bonded to the surface of the compressor shell. However, this method becomes cumbersome and expensive for large and complex systems with a lot of radiating surfaces to be controlled. In the second approach the vibrations are actively blocked in the structural transfer paths. Pinte et al. [1] and Stallaert et al. [4] proposed to integrate a pair of piezo actuators into an existing bearing to introduce control forces directly to a rotating shaft, such that the disturbance is blocked in the force transmission path towards frame and the noise radiating surfaces. This approach has also been investigated in [5], where four magnetostrictive actuators are mounted around a bearing on the input shaft to cancel the vibration at the feet of the gearbox. As a consequence, a noticeable noise reduction of 5-10 dB was obtained. However the installation of the active element in the force transmission path also decreases the system's stiffness.

Therefore the goal of this research is to develop an active system which generates secondary forces directly on the shaft without affecting the system's stiffness. To this end, an axisymmetric piezo based

rotational inertia shaker has been developed, which can be installed directly on the shaft as an add-on device parallel to the functional bearings. The developed shaker is installed in parallel, but close to a functional bearing in order to limit the force transmission through the bearings to the frame.

In addition to the design of the actuator and its placement at the appropriate location, an important step in the design of an active system is the development of a suitable control approach. Both active and (adaptive-) passive methods are often used to control piezo-electric systems. Active methods require an external electric energy source to power the control circuitry and the actuators. As a consequence, the implementation cost is quite high and the system may become unstable. An alternative is to use passive electric networks to control the piezo-element and to realize an acceptable control performance.

By connecting a series connection of an inductor and a resistance to the electrodes of the piezo element, an electromechanical vibration damper or vibration absorber can be created. This methodology is commonly referred to as passive shunt damping. Passive shunt damping is regarded as a simple, low cost, lightweight and easy to implement alternative for active control. N. W. Hagood et al. [7] presented the potential performance of different passive piezo shunt circuits to damp the vibration of a vibrating beam. In analogy to mechanical absorbing systems, where the vibration reduction increases and the controlled frequency range narrows with decreased damping, strong vibration reduction in a small frequency band can be achieved by connecting only an inductance to a piezo with an unavoidable but low internal resistance in series. This inductance creates in combination with the inherent capacitance of the piezo an electrical resonance, which can be tuned so that the piezo elelment acts as a tuned vibration energy absorber at a certain frequency. A J Fleming et al. [8] analyzed the possibility of using a synthetic inductance implemented on a DSP system, as a piezoelectric shunt circuit. For the implementation of this synthetic inductance the transfer functions of the shunted system need to be identified, which makes this technology not applicable for the control of complex systems. De Marneffe et al. [9] and Niederberger et al. [10] proposed to use analog technologies to realize a virtual inductance for a piezo element. Their work focused on increasing the system's damping, while this paper explores the application of piezo shunt control for vibration absorption.

In the following section of this paper, the design of this piezo based inertia shaker is presented. This section also describes the experimental test bed, which is used to evaluate the performance of the inertia shaker. In the third section, a simplified lumped parameter model of the test bed with the inertia shaker is derived. This model is used to demonstrate the theoretically achievable performance of the inertia shaker. In this section also some guidelines are derived to design the virtual shunt inductance. Experimental results are presented in the fourth section. The last section summarizes the main conclusions of the paper.

2 Design of piezo based rotational inertia shaker

The idea behind the design of the piezo based rotational inertia shaker is to use a piezostack actuator to introduce a force between a ring-shaped mass and a rotating element (e.g. a shaft). By accelerating the ring-shaped mass, compensating forces can be generated on the shaft such that shaft vibrations are suppressed. Figure 1 (a) and (b) show a drawing and a photo of the developed prototype of the inertia shaker. In this shaker the Piezomechanik HPSt 150/20 actuator is used. Although the piezo actuator has a sufficient stroke to compensate the disturbances on the test bed, it is acknowledged that in stiff industrial applications, which are excited by larger forces, longer piezo actuators with larger sections should be used to generate the required strokes. The piezo actuator is preloaded by a screw, such that it is capable of applying bi-directional (push/pull) forces. In order to avoid bending of the piezostack, four Z shaped springs were foreseen at each corner, with the actuator centrally located. In the Z shaped spring, the vertical links are much shorter and, more importantly, thicker than the horizontal links such that a high rotational stiffness and a low horizontal stiffness is realized.

In order to evaluate its practical performance, the developed piezo based inertia shaker is tested on an experimental test bed which is shown in Figure 2. In this test bed, a motor drives a shaft, which is supported in a frame by a cylindrical bearing at one side and a double angular contact ball bearing at the other side. The inertia shaker is installed on the shaft close to this latter bearing. Around this bearing, a

ring-shaped module is placed in which two piezo sensors are installed to measure the transmitted force through the bearing in the horizontal and the vertical direction.

A disturbance force on the shaft is induced by an electrodynamic shaker, which is attached to the shaft through a roller bearing. This force generates vibrations in the shaft as well as in the frame. As a result, noise is also radiated by a plate that is attached to the frame. The dimensions of the different parts are chosen such that the test bed has a representative dynamic and acoustic behavior for industrial rotating machinery such as gearboxes.

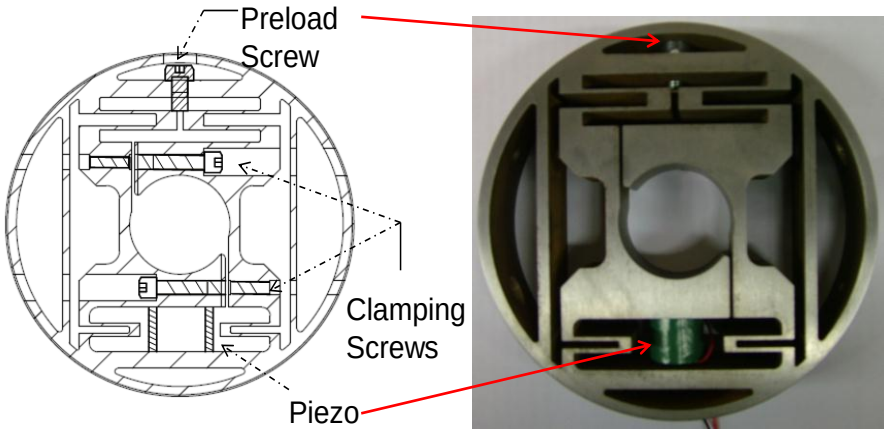

Figure 1: The developed 1D piezo based absorber: a) drawing and b) picture

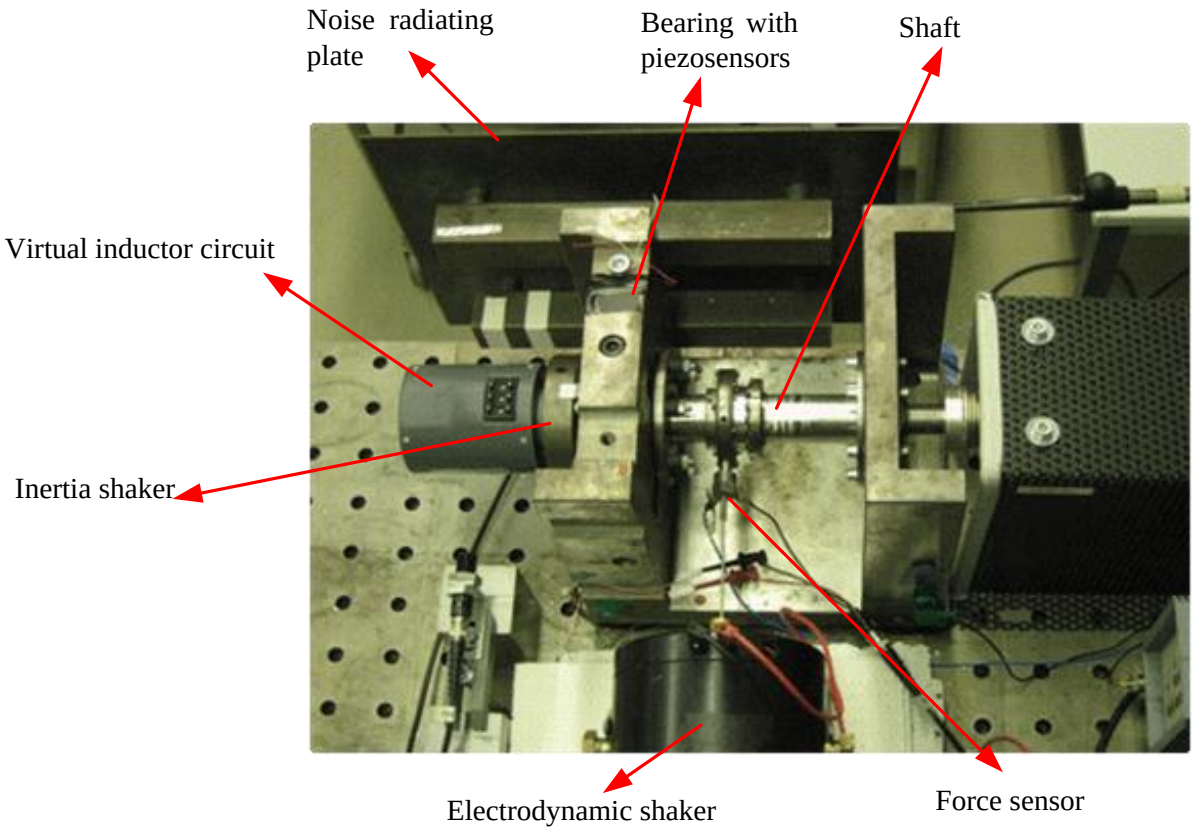

Figure 2: The experimental set up for evaluating the performance of the developed 1D inertia shaker

3 Modeling and work principle

3.1 Model of the test rig

Fig. 3 (a) presents a simplified lumped parameter mechanical model of the set-up, which is an extension of the model in [1] with the dynamics of the inertia shaker. The disturbance force F_s, which stems for example from gear meshing or unbalance forces, is acting on the shaft, represented by the mass m_s. As a consequence, a force is transmitted through the bearings from the shaft to the frame. This frame, represented by the mass m_f, is supported by compliant rubber mounts, modeled by the spring k_o. For the piezo elements used in the system, equivalent mechanical and electrical models derived in [11] are used. The stiffness of the bearing with the piezosensors is labeled as k_{b1}, stiffness k_s in series with k_{b1} represents the piezosensor, while the stiffness of the second bearing is labeled as k_{b2}.The ring shaped mass of the inertia shaker is modeled as a discrete m_t, connected to the shaft by two springs k_m and k_e, which are the mechanical and electrical stiffness of the piezo actuator. The electrical stiffness k_e is inversely proportional to the internal capacitance of the piezo actuator. F is the force generated by the piezo actuator, which is proportional to the voltage over its electrodes. The voltage to the electrodes of this piezo actuator is represented by an equivalent force F. The plate is modeled by spring k_p and mass m_p.

From this model, it is clear that the total transmitted force between the shaft and the frame consists of the measured force through the bearings and the inertia shaker. Reduction of the noise radiation from the plate can be achieved when the shaft vibrations are reduced, as consequently also the force transmitted through the bearing will decrease.

In order to interpret the effect of connecting a shunt circuit to the piezoelement, an equivalent electrical model of the mechanical model is derived in Figure 3 (b). To build this model, the relation between mechanical parameters and electrical parameters as defined in [11] is used. Since the disturbance force in rotating machinery is typically periodic, the idea is to connect an inductance to the piezo in order to create a vibration absorber at the disturbance frequency. As the shaft acceleration and the transmitted force through the bearing with piezosensors are a good measure of the performance of the inertia shaker, the objective in the selection of the inductance value is to minimize the shaft vibrations, which is equivalent to the minimization of the current through the inductor m_s. Ideally, no current flows through the inductors m_s and m_f when the total impedance of the subcircuit (m_t, k_m, Z, C_e) is infinitely high. It can be derived that this ideal case is obtained when the impedance Z connected to the electrodes of the piezoactuator is equal to:

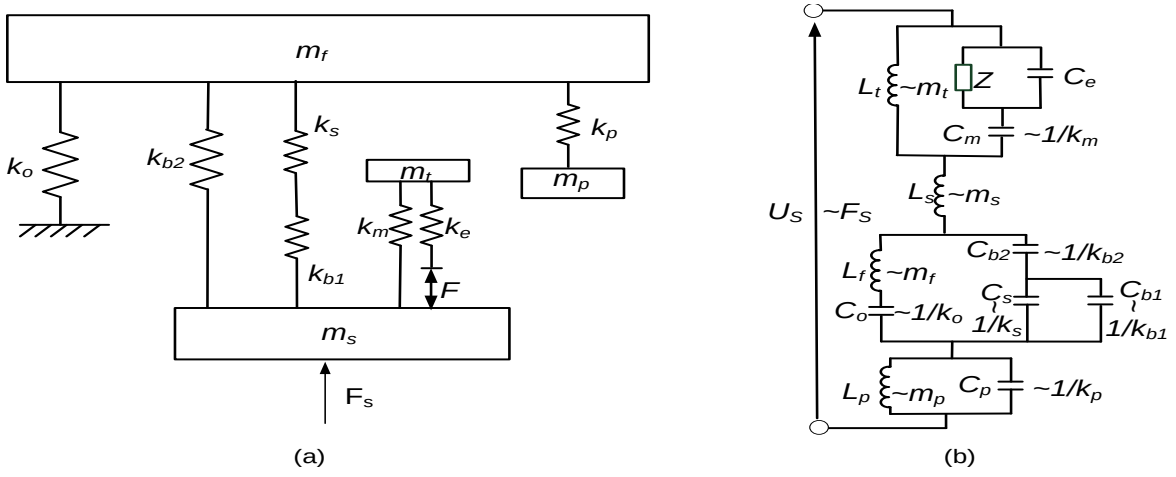

Figure 3: (a) The simplified mechanical model of the test bed, (b) The equivalent electrical circuit for the test bed.

$$Z = -\frac{1+s^2 L_t C_m}{s(C_m + C_e)(1+s^2 L_t \dfrac{C_m C_e}{C_m + C_e})} \tag{3.1}$$

Since the stiffness of the piezo element is very high, the frequency of the disturbance force will typically be lower than the mechanical resonance frequency determined by (k_m, m_t). From the equation (3.1), it can be seen that in this case the ideal impedance can be approximated as a negative capacitance:

$$C_{ideal} = -\frac{1}{C_m + C_e} \tag{3.2}$$

where the summation of C_m and C_e is equal to the capacitance of the piezoelectric actuator under constant mechanical stress [11], the value of which is equal to 2.6 μF in this case. At a single frequency this negative capacitance can be implemented as an inductance:

$$L_{ideal} = \frac{1}{\omega^2 (C_m + C_e)} \tag{3.3}$$

When the frequency of the disturbance is changing, a variable inductance is needed to realize an adaptive vibration absorber, which is difficult to realize with hardware components. Therefore, the potential of using a virtual inductor circuit based on electronic components has been explored.

3.2 Working principle of the virtual inductor circuit

Antoniou's gyrator circuit [10] can be used to implement a variable inductance, which consists of operational amplifiers and passive electrical components, is shown in Figure 3.2. However its application is limited because of its large internal resistance. This section will illustrate how to choose the circuit parameters to improve its performance.

In the following analysis of the virtual inductor in Figure 3.2, it is assumed that the operational amplifiers (OpAmps) have finite open loop gains (A_1 and A_2) and that their input currents are still zero. Then the system matrix equation that describes this circuit is given by

$$\begin{bmatrix} R_1 & \dfrac{1}{j\omega C} & 0 & -1 & 0 \\ 0 & -R_2 & -R_3 & 0 & -1 \\ 1 & 0 & R_4 & 1 & -1 \\ R_1 & 0 & 0 & 0 & A_2 \\ 0 & 0 & R_3 + R_4 & -A_1 & 0 \end{bmatrix} \begin{bmatrix} I_{in} \\ I_2 \\ I_3 \\ U_{e1} \\ U_{e2} \end{bmatrix} = \begin{bmatrix} 0 \\ 0 \\ 1 \\ 1 \\ 0 \end{bmatrix} U_{in} \tag{3.4}$$

By solving this linear matrix equation, the input impedance of the virtual inductor circuit is derived:

$$Z_{in} = \frac{U_{in}}{I_{in}} = \frac{j\omega C R_1 R_2 R_4 A_1 A_2 + j\omega C R_1 R_2 (R_3 + R_4)(A_2 + 1) + R_1 (R_3 + R_4)(A_2 + 1)}{R_3 A_1 A_2 + (A_1 + 1)(R_3 + R_4) + j\omega R_2 C (A_2 + 1)(R_3 + R_4)} \tag{3.5}$$

In the case that A_1 and A_2 are equal to infinite, a perfect inductance is realized:

$$\lim_{(A_1, A_2) \to \infty} Z_{in} = \frac{U_{in}}{I_{in}} = \frac{j\omega C R_1 R_2 R_4}{R_3} = j\omega L, \tag{3.6}$$

with $L=CR_1R_2R_4/R_3$. However, the gains of real OpAmps are not infinite, therefore the phase angle of the input impedance in equation (3.5) will always be smaller than 90˚, which means that the real impedance of the virtual inductor in Figure 4 does not only consist of an inductance , but also a series resistance. This internal resistance will limit the absorbing performance, and should therefore be kept as small as possible.

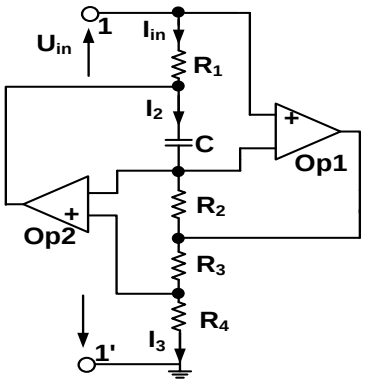

Figure 4: Antoniou's virtual inductor circuit

The tangent of the phase angle θ of the input impedance is given by equation (3.7) and should approach infinity for a minimal internal resistance.

$$\tan(\theta)=\frac{\omega CR_2+\frac{\omega CR_2R_4A_1A_2}{(R_3+R_4)(A_2+1)}-\frac{\omega R_2C(R_3+R_4)(A_2+1)}{R_3A_1A_2+(R_3+R_4)(A_2+1)}}{1+(\omega CR_2+\frac{\omega CR_2R_4A_1A_2}{(R_3+R_4)(A_2+1)})(\frac{\omega R_2C(R_3+R_4)(A_2+1)}{R_3A_1A_2+(R_3+R_4)(A_2+1)})} \tag{3.7}$$

Since A_1A_2 is much larger than (A_1+1), the expression in equation (3.7) can be simplified:

$$\tan(\theta)=\frac{\omega CR_2A_1}{1+\frac{(\omega CR_2)^2R_4}{R_3}+\frac{R_3}{R_4}+(\omega CR_2)^2} \tag{3.8}$$

To get the maximum value in equation (3.8), the partial derivative of $\tan(\theta)$ with respect to the ratio of R_3 and R_4 is calculated:

$$\frac{\partial\tan(\theta)}{\partial(\frac{R_3}{R_4})}=\frac{-\omega CR_2A_1(1-\frac{(\omega CR_2)^2R_4^{\,2}}{R_3^{\,2}})}{(1+\frac{(\omega CR_2)^2R_4}{R_3}+\frac{R_3}{R_4}+(\omega CR_2)^2)^2} \tag{3.9}$$

$\tan(\theta)$ is maximized when $\frac{\partial\tan(\theta)}{\partial(\frac{R_3}{R_4})}=0$, which is realized when

$$\frac{R_3}{R_4}=\omega CR_2 \tag{3.10}$$

The corresponding maximum value of $\tan(\theta)$ is:

$$\max\tan(\theta)=\max\left(\frac{\omega CR_2A_1}{1+\frac{(\omega CR_2)^2R_4}{R_3}+\frac{R_3}{R_4}+(\omega CR_2)^2}\right)=\max\left(\frac{\omega CR_2A_1}{(1+\omega CR_2)^2}\right) \tag{3.11}$$

The partial derivative of $\tan(\theta)$ with respect to the product of ω, C and R_2 is given by

$$\frac{\partial\tan(\theta)}{\partial(\omega CR_2)}=\frac{(1-\omega CR_2)A_1}{(1+\omega CR_2)^3} \tag{3.12}$$

$\tan(\theta)$ is maximized when $\frac{\partial\tan(\theta)}{\partial(\omega CR_2)}=0$, which is realized when,

$$\omega CR_2=1 \tag{3.13}$$

If equation (3.10) and (3.13) are satisfied, the following maximum object value of $\tan(\theta)$ is reached,

$$\max\tan(\theta)=\frac{A_1}{4} \tag{3.14}$$

Based on the above analysis, it is possible to minimize the internal resistance by carefully selecting the circuit parameters according to the following rules:

1) The product of ω, C and R_2 should be equal to one;
2) R_3 should be equal to R_4.

However, there are at least three circuit parameters that need to be adaptive in order to keep in the point of minimal resistance when the frequency varies. In this paper, only R_4 is made adaptive, while the other parameters are fixed. The product of R_2 and C are set close to one, and R_3 is selected to let R_4 perform in an appropriate range.

An additional requirement of the virtual inductor circuit is that the output voltages of the operational amplifiers in the Figure 3.2 should be within the bounds of the power supplier. These output voltages can be calculated based on the following equations. The notations I_{in} and L represent the current flowing to R_1 and the ideal value of the virtual inductance respectively.

$$U_{op1}=-I_{in}R_1*j\omega CR_2+I_{in}*j\omega L \tag{3.15}$$

$$U_{op2}=-I_{in}R_1+I_{in}*j\omega L \tag{3.16}$$

At one specific frequency, the output voltages of the OpAmps are mainly determined by the product of R_1 and I_{in} since ω and L are fixed. To avoid saturation of the OpAmps, R_1 should be set to a small value.

4 Experiment and results

This section describes the experiments that have been carried out to validate the practical applicability of the virtual inductor circuit. The experiments have been carried out in two conditions: (i) when the shaft is not rotating and (ii) when the shaft is rotating.

4.1 Experimental results for a non-rotating shaft

4.1.1 Impedance calculation of the virtual inductor circuit

In this section, the tuning procedure of the virtual inductance developed in section (3.2) is validated. The aim of the experiment is to demonstrate that internal resistance of the virtual inductor varies with respect

to different circuit parameters. Depending on the values of the electrical components in the virtual inductor circuit, the achieved vibration reductions will be different.

Two configurations of the virtual inductor circuit have been composed, which are shown in table 1. By adapting the value of R_4, the virtual inductance can be adjusted depending on the vibration disturbance frequency.

Circuit parameters	R1 (ohm)	R2 (ohm)	R3 (ohm)	R4 (ohm)	C (μF)
Configuration 1	100	1000	100	potentiometer	0.01
Configuration 2	18	1000	86	potentiometer	0.1

Table 1: Virtual inductor circuit parameters

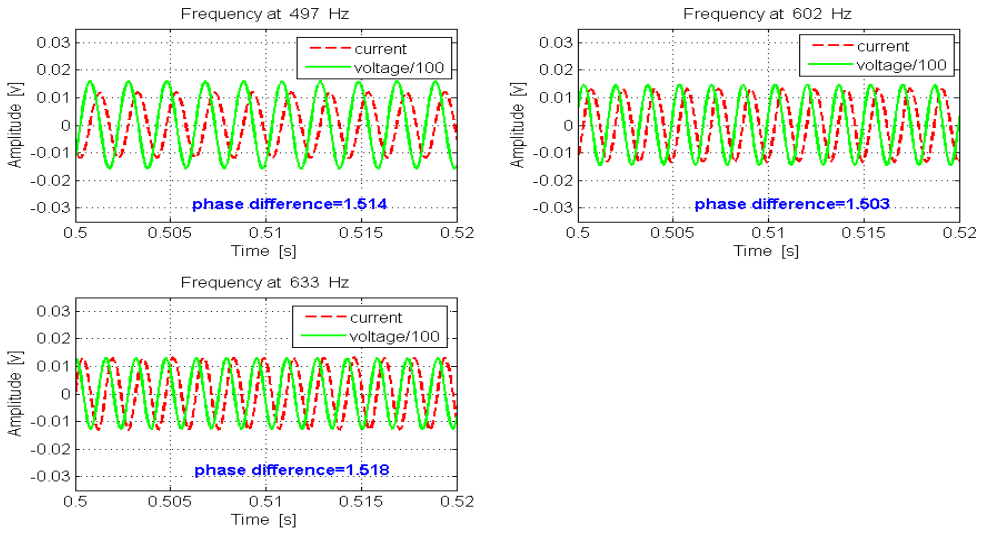

Figure 5: The voltages and currents over the piezo electrodes at different target frequencies, where the virtual inductor circuit is built in configuration 1.

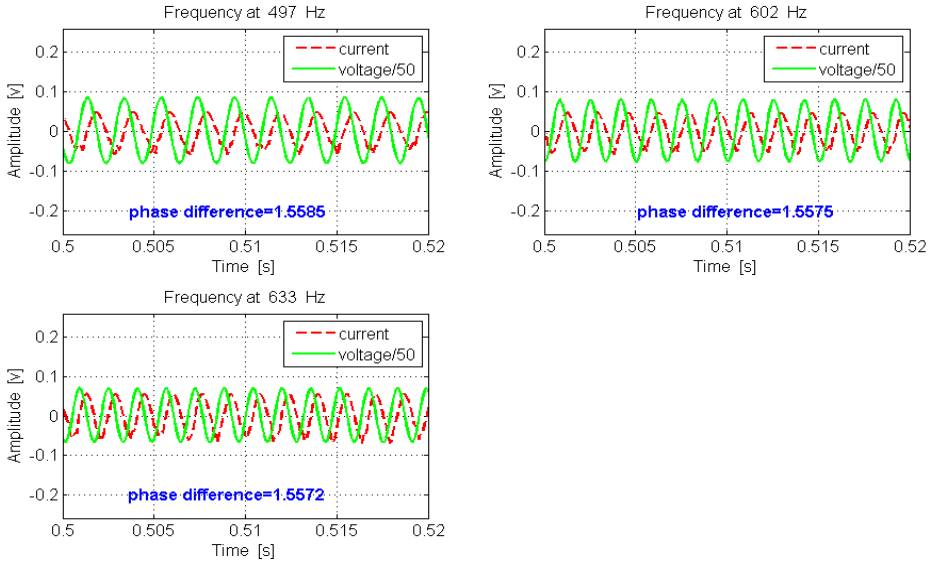

Figure 6: The relation between the voltages and currents over the piezo electrodes at different target frequencies, where the virtual inductor circuit is built in configuration 2.

Three sets of experiments have been performed to compare the internal resistance of the virtual inductor circuit at different frequencies. In each set, a sinusoidal disturbance force is applied. The voltage and the current are measured when the highest vibration reduction is achieved. Figure 5 presents the phase difference between the voltage and the current of the virtual inductor circuit composed in configuration 1, while the corresponding results of the circuit built in configuration 2 are shown in Figure 6. It can be seen that the phase angles in configuration 2 are more approaching the ideal phase angle $\pi/2$, which means that the internal resistance of the virtual inductor circuit composed in configuration 2 will be smaller than the value in configuration 1.

The real impedances of the virtual inductor circuits as well as the achieved shaft vibration reductions are shown in table 2, which confirm that the internal resistance can be decreased by carefully selecting the circuit parameters and consequently a larger vibration reduction can also be obtained. Additionally, the values of the function $\tan(\theta)$ in equation (3.7) for the circuit parameters in configuration 1 and 2 are presented, where A represents the open loop gain of the OpAmp. Although the maximum value of $\tan(\theta)$ derived in equation (3.14) is not reached due to the selection of a small value of R_1, the internal resistance of the proposed virtual inductor circuit has already been quite small such that a vibration reduction of at least 12 dB can be obtained.

Description	Frequency(Hz)	497	602	633
Configuration1	L (H)	0.0416	0.0282	0.0247
	R (ohm)	7.4442	5.2535	5.1823
	Reduction (dB)	3.001	4.495	1.281
	$f(R_1,R_2,R_3,R_4,C)$	0.0293*A	0.0351*A	0.0368*A
Configuration2	L (H)	0.0392	0.0268	0.0242
	R (ohm)	1.5102	1.3446	1.3061
	Reduction (dB)	14.43	20.01	12.41
	$f(R_1,R_2,R_3,R_4,C)$	0.0951*A	0.1130*A	0.1181*A
Equivalent capacitance	$C_e + C_m$ (μF)	2.6	2.6	2.6
Ideal shunt impedance	$1/\omega^2(C_e + C_m)$	0.0395	0.0269	0.0243

Table 2: The real impedance of the virtual inductor circuit and the achievable shaft vibration reductions

4.1.2 Reduction results with a sinusoidal and a broadband excitation

To illustrate the potential of the developed inertia shaker, which is controlled by the proposed virtual inductor circuit, the vibration reduction as well as the noise radiation reduction is measured in case of a sinusoidal disturbance force. In Figure 7, the accelerations at end of the shaft and the plate noise radiation were compared respectively when the optimally tuned virtual inductance was turned off and on for a sinusoidal disturbance force of 497 Hz on the non-rotating shaft. In Figure 8, the frequency of the disturbance force was changed to 602 Hz. It can be seen that the achieved vibration reduction and the corresponding noise reduction are 14 dB and 9 dB respectively at 497 Hz, which means that a cancellation of the shaft vibration leads to a reduction of the noise radiation. An even larger vibration reduction of 19 dB can be realized at 602 Hz, but no significant corresponding audible reduction is observed which is probably due to the fact that this frequency is a dominant shaft resonance with poor plate radiation efficiency.

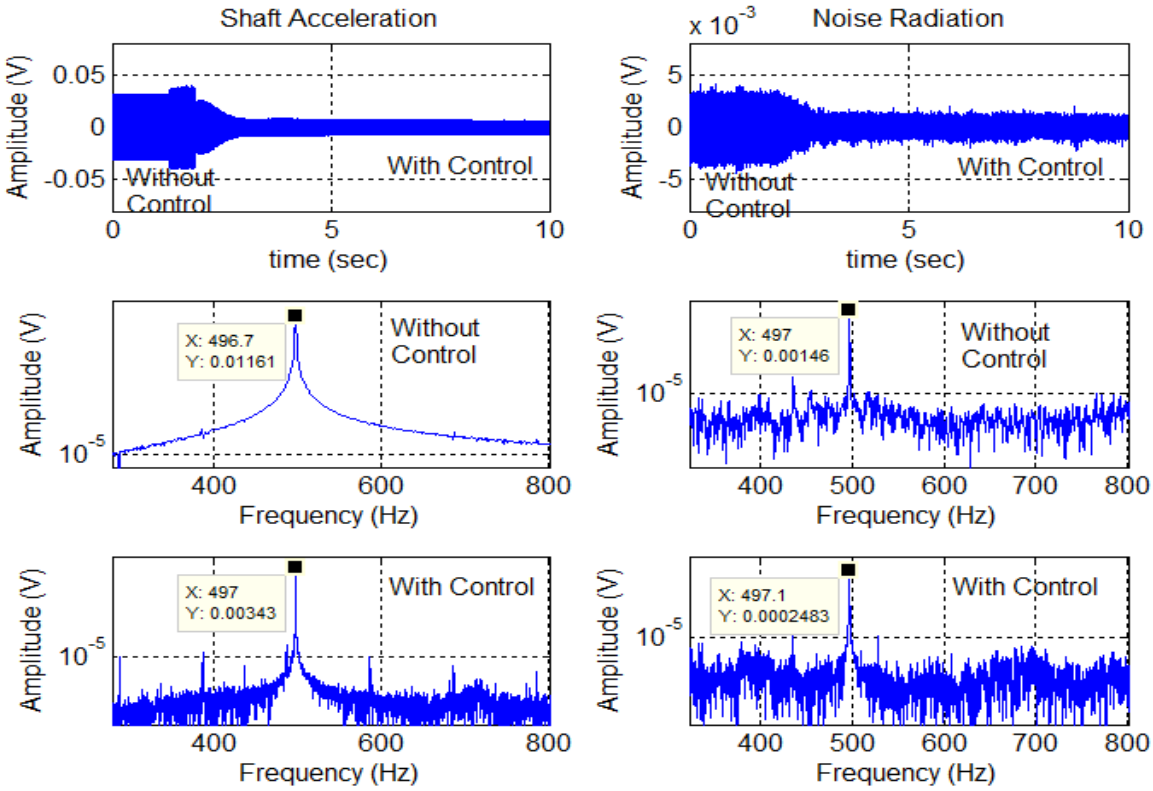

Figure 7: The shaft acceleration and the noise radiation, where the disturbance frequency is 497 Hz

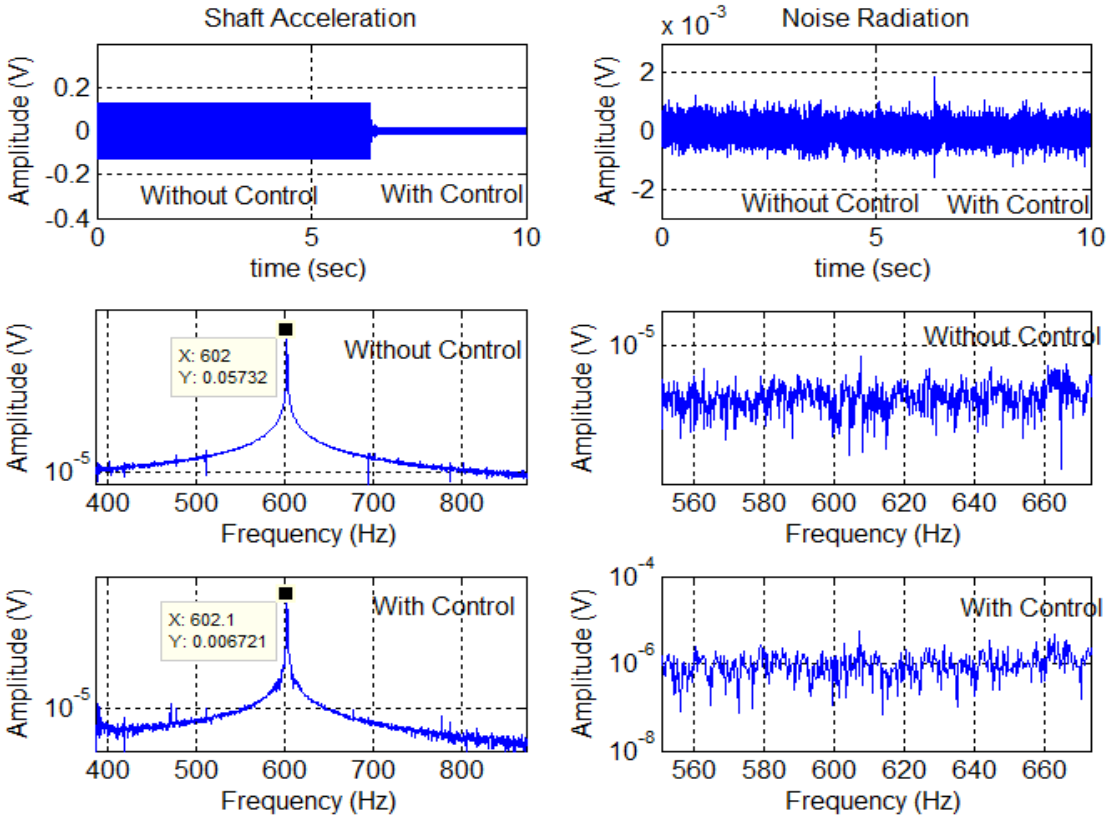

Figure 8: The shaft acceleration and the noise radiation, where the disturbance frequency is 602 Hz

Additionally, to illustrate the working principle of the virtual inductor circuit, the system was also tested when a white noise between 620 Hz and 650 Hz was used as disturbance force. The transfer function between the applied force and the acceleration at the end of the shaft are compared in Figure 9 when the virtual inductance was turned off and tuned to 2 different frequencies. It is clear that, the developed inertia shaker leads to a clear vibration reduction in a narrow frequency range, but also two new resonance frequencies are created. The observations here confirm that the developed inertia shaker realizes the same functionality as tuned inertia mass absorber.

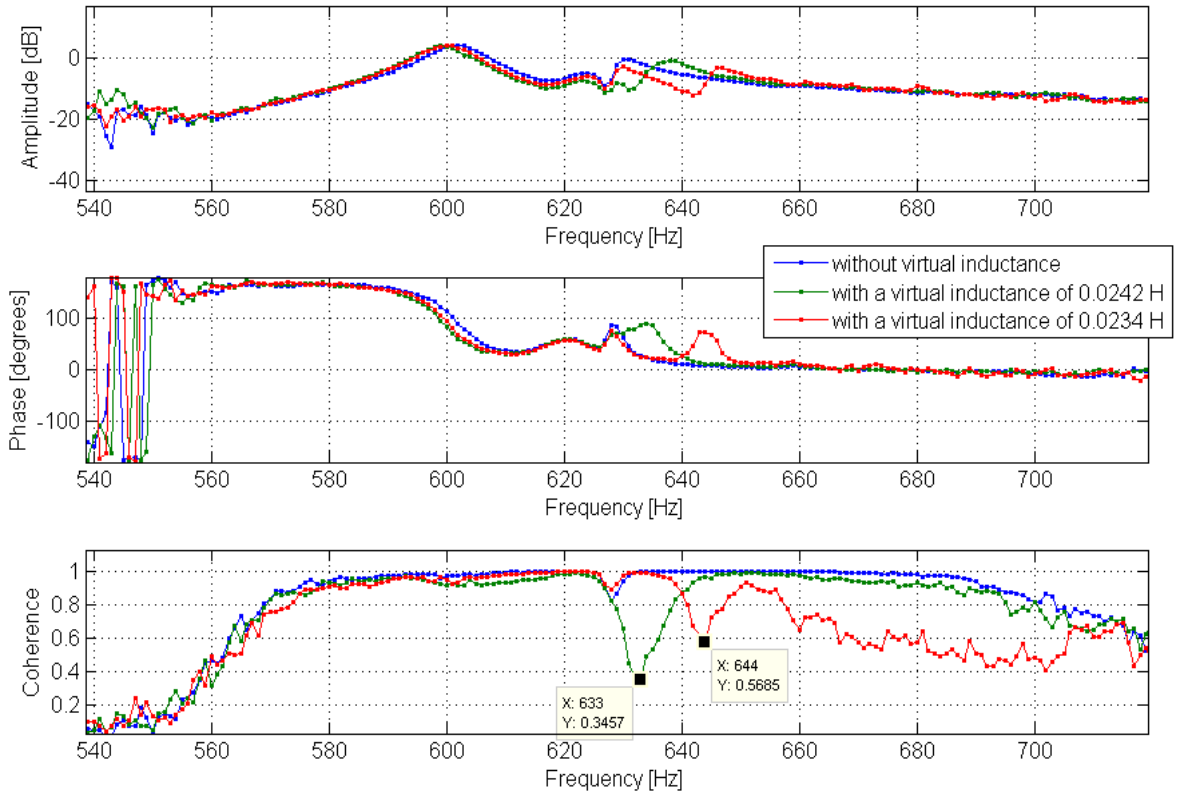

Figure 9: The transfer function between the applied force and the shaft acceleration without virtual inductance, with a virtual inductance of 0.0242 H and with a virtual inductance of 0.0234 H, where the frequency rang is from 620 (Hz) to 650 (Hz).

4.2 Experimental results for a rotating shaft

In this section, experiments with the proposed tunable inductor circuits were performed when the shaft was rotating at 60 rpm. The horizontal piezo-sensor in the bearing is chosen as the error signal to evaluate the performance. While in the non-rotating experiments the piezo shunt circuit was powered by a power supplier, in the rotating experiments a 9V battery and a DC to DC convertor is used to power the circuit.

The experiments have been carried out in four steps, which are described in the table 3. Figure 10 compares the horizontal transmitted forces between the non-rotating shaft and the frame when the virtual inductor is turned off and on as well as the results between the rotating shaft and the frame. The corresponding frequency content of each segment in Figure 10 is shown in Figure 11. It can be seen that a reduction of 20 dB of the transmitted force is obtained when the shaft is not rotating, which confirms the conclusion of the previous section, while the reduction is only around 6 dB at the exciting frequency when the shaft is rotating. Clearly, the conventional Fast Fourier transform (FFT) cannot objectively show the effect of developed the inertia shaker in the rotating test, since it is used to observe the amplitude

difference in frequency domain. Therefore, the time domain signals need to be projected into the angular domain, such that the reduction at each angular position in one rotating circle can be compared.

Experimental steps	Status of shaft	Status of virtual inductor	Disturbance force
Step 1	Not-rotating	Switched off	A sinusoidal signal at 595 Hz
Step 2	Not-rotating	Switched on	
Step 3	Rotating	Switched off	
Step 4	Rotating	Switched on	

Table 3: The experimental procedures

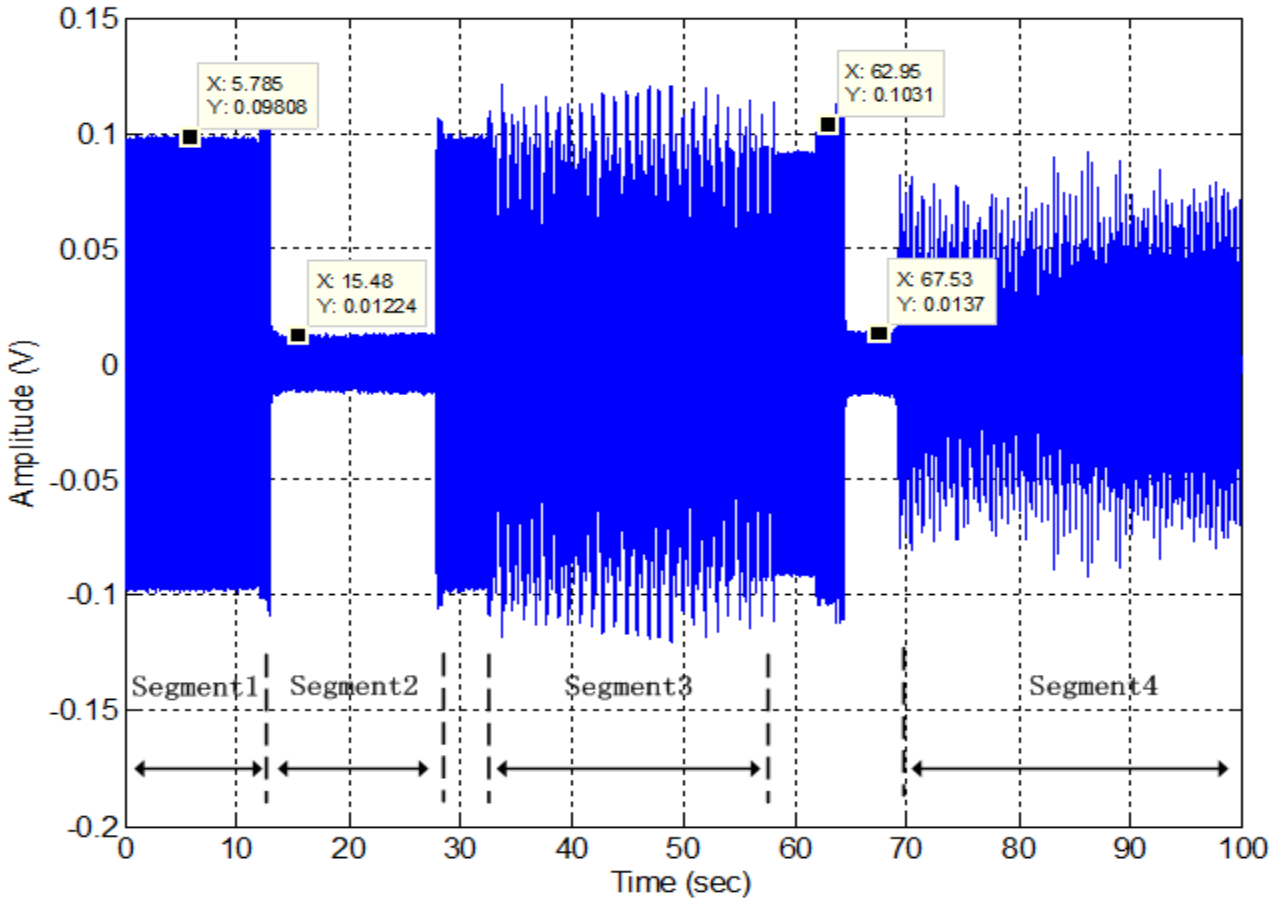

Figure 10: The horizontal transmitted force between the shaft and the frame in time domain.

To this end, a photoelectric switch which delivers one pulse per revolution is introduced to synchronize the force signal and the rotating signal. The achieved reductions in the angular domain are presented in Figure 12, where the different color curves represent different revolutions. It can be seen that the maximum reduction, comparable to the value obtained in the non-rotating test, is obtained when the piezo actuator is in line with the disturbance force, while there is nearly no reduction when the piezo actuator is positioned perpendicular direction to the disturbance. To improve the performance, a second inertia shaker should be installed on the shaft, with its piezo actuator in a perpendicular direction compared to the piezo actuator in the first inertia shaker.

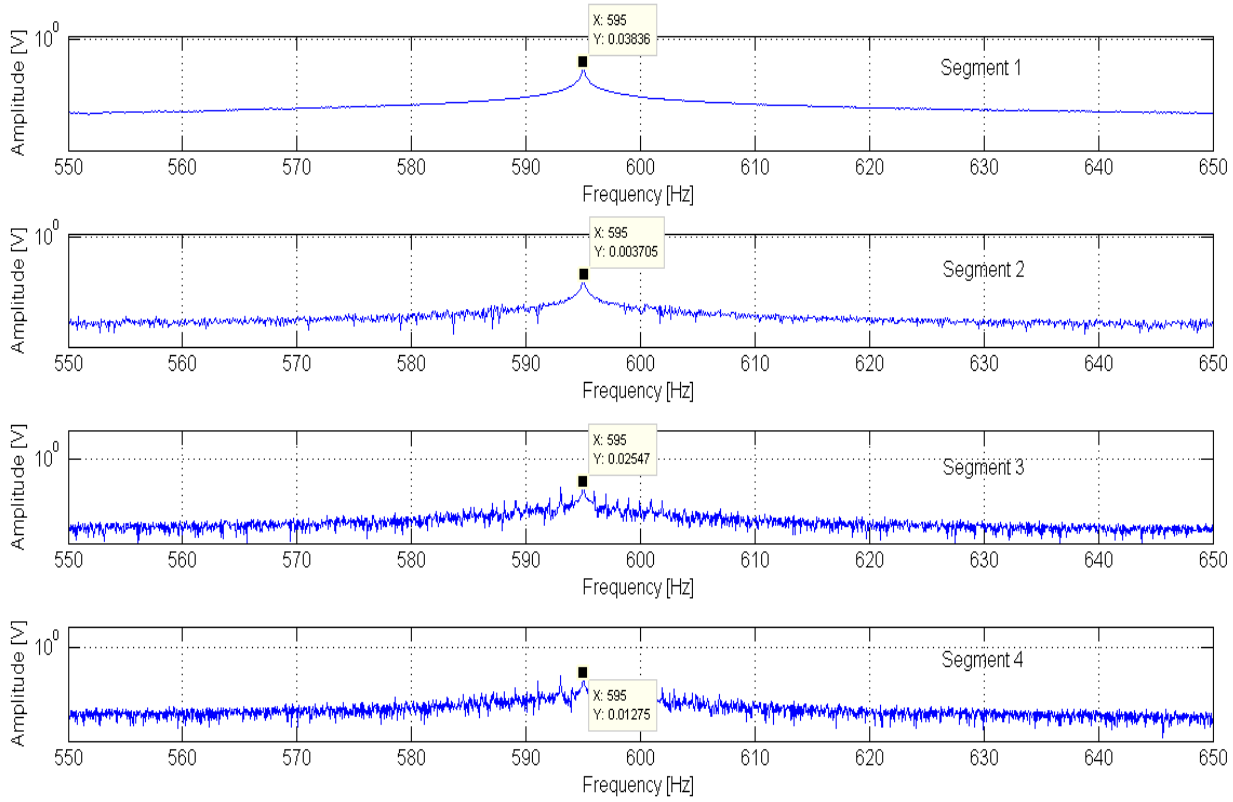

Figure 11: The corresponding spectra of the signals in Figure 4.6.

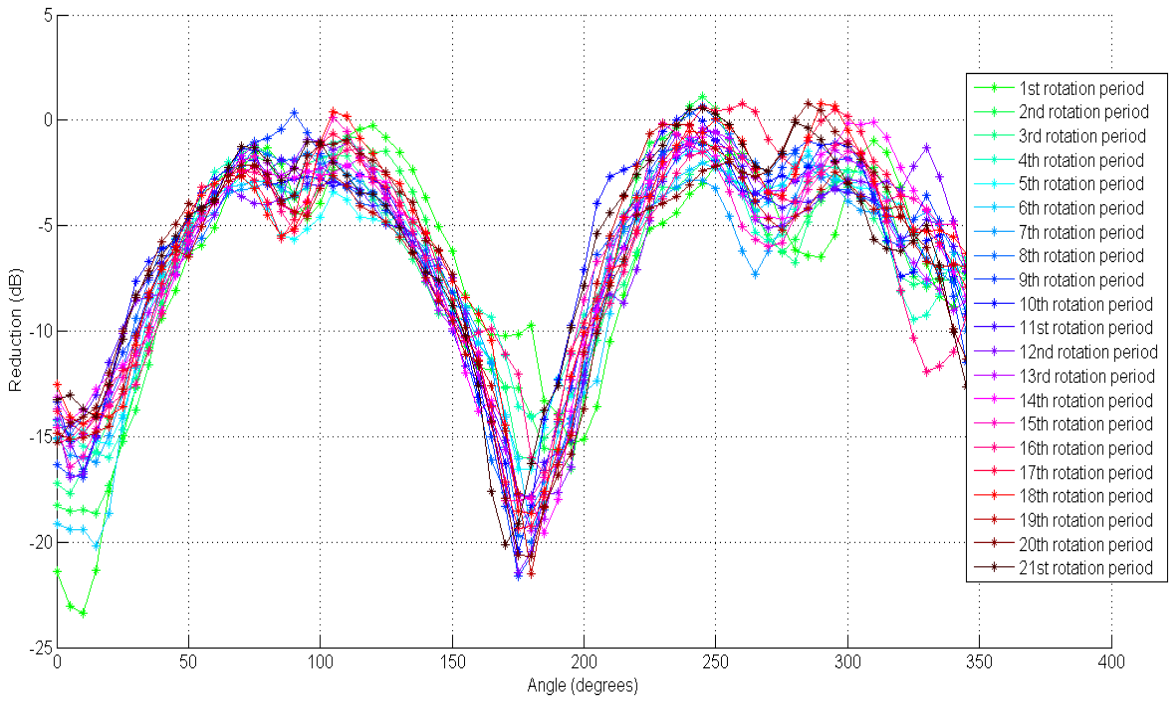

Figure 12: The achieved reductions in the angular domain, the different color curves represent different rotating periods.

5 Conclusion

In this paper, a modular piezo based adaptive absorber has been developed, which can be mounted on a rotating shaft to reduce the vibrations. As an add-on device, it will not impact the static strength or stiffness of the host structure. This adaptive absorber has been tested on an experimental test bed. When it is optimally tuned, a reduction of the shaft vibration of more than 12 dB was achieved in the non-rotating tests. Comparable reductions were obtained on a rotating shaft when the piezo actuator is aligned with the disturbance force. This demonstrates the technical feasibility of suppressing rotating shaft vibrations by using piezo based inertia shaker. Since the developed prototype consists of one piezo element that can only generate forces in one direction, future work consists of the design and control of a 2-dimensional axisymmetric rotational inertia shaker, which can generate shaft forces in two radial directions.

References

[1] G. Pinte, S. Devos, B. Stallaert, W. Symens, J. Swevers and P. Sas, *A piezo-based bearing for the active structural acoustic control of rotating machinery*, Journal of Sound and Vibration, 2009

[2] Gardonio P. and Elliott S.J., *Smart panels for active structural acoustic control*, Smart Materials and structures, 12(6) (2004): 1214-1336.

[3] A. R. Masters, S. J. Kim and J. D. D. Jones, *Active control of compressor noise radiation using piezoelectric actuators*, International Compressor Engineering Conference, Paper 822,1992

[4] B. Stallaert, *Active structural acoustic source control of rotating machinery*, Ph.D. Thesis, KU Leuven, Department of Mechanical Engineering, Division of Production Engineering, Machine Design and Automation, 2010.

[5] B. Rebbechi, C. Howard and C. Hansen, *Active control of gearbox vibration*, In Proceedings of Active 99, pages 295–303, December 1999.

[6] M. A. Franchek, M. W. Ryan and R. J. Bernhard, *Adaptive passive vibration control*, Journal of Sound and Vibration(1995) 189(5),565-585.

[7] N. W. Hagood, A. H. von Flotow, *Damping of structural vibrations with piezoelectric materials and passive electrical networks*, Journal of Sound and Vibration, 146 (2) (1991) 243–268.

[8] A. J. Flemin, S. O. R Moheimani, *Adaptive piezoelectric shunt damping*, Smart Materials and Structures, structures 12 (2003) 36-48.

[9] B. deMarneffe, *Active and Passive Vibration Isolation and Damping via Shunted Transducers*, PhD. thesis, ULB, Department of Mechanical Engineering and Robotics, Active Structures Laboratory,2007

[10] D. Niederberger, *Smart Damping Materials using Shunt Control*, PhD. thesis, Swiss Federal Institute of Technology (ETH) Zurich, 2005.

[11] S. Devos, *Development of fast, stiff and high-resolution piezoelectric motors with integrated bearing driving*, PhD. thesis, KU Leuven, Department of Mechanical Engineering, Division of Production engineering, Machine design and Automation, 2006

[12] M. Date, M. Kutani, S. Sakai, *Electrically controlled elasticity utilizing piezoelectric coupling*, Journal of Applied Physics, Volume 87 (2000), Number 2.